J. Am. Soc. Mass Spectrom. (2017) 28:1160–1165
DOI: 10.1007/s13361-017-1645-8

FOCUS: HONORING R. G. COOKS' ELECTION TO THE NATIONAL ACADEMY OF SCIENCES: RESEARCH ARTICLE

Characterization of ZnO Nanoparticles using Superconducting Tunnel Junction Cryodetection Mass Spectrometry

Logan D. Plath,[1,2] Zongyu Wang,[2] Jiajun Yan,[2] Krzysztof Matyjaszewski,[2] Mark E. Bier[1,2]

[1]Center for Molecular Analysis, Department of Chemistry, Carnegie Mellon University, 4400 Fifth Ave., Pittsburgh, PA 15213, USA
[2]Department of Chemistry, Carnegie Mellon University, 4400 Fifth Ave., Pittsburgh, PA 15213, USA

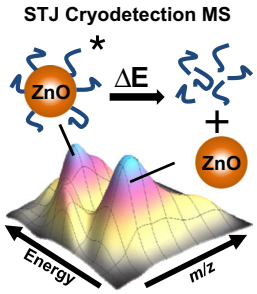

Abstract. Zinc oxide (ZnO) nanoparticles coated with either *n*-octylamine (OA) or α-amino poly(styrene-*co*-acrylonitrile) (PSAN) ligands (L) have been analyzed using laser desorption/ionization and matrix assisted laser desorption/ionization (MALDI) time-of-flight (TOF) superconducting tunnel junction (STJ) cryodetection mass spectrometry. STJ cryodetection has the advantage of high *m*/*z* detection and allows for the determination of average molecular weights and dispersities for 500–600 kDa ZnO-L nanoparticles. The ability to detect the relative energies deposited into the STJs has allowed for investigation of ZnO-L metastable fragmentation. ZnO-L precursor ions gain enough internal energy during the MALDI process to undergo metastable fragmentation in the flight tube. These fragments produced a lower energy peak, which was assigned as ligand-stripped ZnO cores whereas the individual ligands were at too low of an energy to be observed. From these STJ energy resolved peaks, the average weight percentage of inorganic material making up the nanoparticle was determined, where ZnO-OA and ZnO-PSAN nanoparticles are comprised of ~62% and ~68% wt ZnO, respectively. In one example, grafting densities were calculated based on the metastable fragmentation of ligands from the core to be 16 and 1.1 nm^{-2} for ZnO-OA and ZnO-PSAN, respectively, and compared with values determined by thermogravimetric analysis (TGA) and transmission electron microscopy (TEM).

Keywords: ZnO, ZnO nanoparticles, Nanocrystals, STJ, Cryodetector, STJ cryodetector, Superconducting tunnel junction, Metastable fragmentation, Ligand loading

Received: 28 December 2016/Revised: 26 February 2017/Accepted: 27 February 2017/Published Online: 18 April 2017

Introduction

Zinc oxide (ZnO) nanoparticles have received significant attention in the field of nanotechnology due to the unique optical and electronic properties associated with these structures [1, 2]. For example, ZnO nanoparticles have been incorporated into textile construction for UV protection properties and also in inorganic-polymer photovoltaic cells as ultra-fast charge carriers [3, 4]. For these inorganic-polymer nanocomposite hybrids, researchers are often concerned about the structure, size distribution, stability, and degree of surface modification of particles. Characterization of these heterogeneous nanoparticles, where the above measurements can be made accurately and efficiently, would greatly help to advance the field. The use of a specialized mass spectrometry (MS) method using cryodetection is shown here as a new tool to improve such nanoparticle characterization.

Cryodetection MS was first introduced by Twerenbold and coworkers in 1996 by coupling a superconducting tunnel junction (STJ) to a matrix-assisted laser desorption ionization (MALDI) time-of-flight (TOF) mass spectrometer [5]. They demonstrated high *m*/*z* analysis sensitivity, where ion velocity dependence of conventional detectors show reduced signal response [6, 7]. Since then, results have been obtained using STJ cryodetection for ultra-high mass macromolecules such as 13 MDa bacteriophage capsids, 2 MDa polystyrene, von

Electronic supplementary material The online version of this article (doi:10.1007/s13361-017-1645-8) contains supplementary material, which is available to authorized users.

Correspondence to: Mark E. Bier; *e-mail:* mbier@andrew.cmu.edu

Willebrand factor (1.5 MDa), IgM (1 MDa), and heterogeneous systems such as ferritin (~850 kDa) [8–11].

In this report, ZnO nanoparticles (~5 nm in diameter) attached with protecting ligands (L): *n*-octylamine (OA, MW=129 Da) and a synthetic copolymer, *α*-amino poly(styrene-*co*-acrylonitrile) (PSAN, M_n=1500 Da), were analyzed at low charge states by laser desorption ionization (LDI) and MALDI-TOF cryodetection MS. As demonstrated herein, there is analytical utility when studying these large heterogeneous nanoparticles at low-charge states with STJ cryodetectors. Determining the molecular weight of these large, heterogeneous particles at high charge may also be possible, but would require resolving individual charge states at high resolution. Since these ZnO nanoparticles are disperse, this may not be readily obtainable. In this work, in addition to determining the mass and dispersity of theses ZnO-L nanoparticles, the energies deposited into the STJ cryodetector are used to measure metastable fragment masses. The capability of making these energy measurements, unique to STJ MS, are investigated for the quantification of ligand loading on the ZnO nanoparticle surface.

Experimental

Materials and Synthesis

Zinc(II) 2-ethylhexanoate and tris(2-dimethylaminoethyl)amine (Me_6TREN) were obtained from Alfa Aesar (Haverhill, MA, USA). Styrene (St), acrylonitrile (AN), diphenyl ether, *n*-octylamine (OA), triethylamine TEA), α-bromoisobutyryl bromide (BiBB), sodium bicarbonate ($NaHCO_3$), copper(II) bromide ($CuBr_2$), tin(II) 2-ethylhexanoate ($Sn(EH)_2$, hydrazine, sinapinic acid (SA), and monoclonal immunoglobulin G1 (IgG1) were obtained from Sigma-Aldrich (St. Louis, MO, USA). N-(2-hydroxyethyl)phthalimide (NHP) was obtained from Acros (Fair Lawn, NJ, USA). Tetrahydrofuran (THF) was obtained from VWR (Radnor, PA, USA) and Fisher Scientific (Fair Lawn, NJ, USA). Additional solvents: acetonitrile, ethyl acetate, anisole, dimethylformamide (DMF), dichloromethane, methanol, hexane, acetone, and water were of 99% purity or greater and obtained from VWR (Radnor, PA, USA), Fisher Scientific (Fair Lawn, NJ, USA), or Sigma-Aldrich (St. Louis, MO, USA). ZnO-OA nanoparticles were synthesized as reported by Epifani et al. and Weber et al. [12, 13]. ZnO-PSAN nanoparticles were synthesized from ZnO-OA using a ligand exchange protocol described previously [14]. Details regarding the synthesis of PSAN ligands can be found in the Supplementary Materials.

LDI/MALDI-TOF-STJ MS Experimental Details

All MS data were acquired on a modified Macromizer [10] (Comet AG, Flamatt, Switzerland) incorporating a 3.75 m flight tube. LDI and MALDI experiments were performed in positive ion/linear mode using 20 kV accelerating voltages except where noted. In all experiments, the extraction grid lens was pulsed to 17 kV and the middle element of the Einzel lens was held at 10.25 kV. The extraction delay time was set to 5 μs. The 16-channel STJ array was held at 0.34 K and detectors were biased at 350 μV. For LDI experiments, ZnO-OA (12 mg/mL in THF) and ZnO-PSAN (40 mg/mL in THF) were spotted directly onto the plate and allowed to dry in air prior to introduction into the instrument ion source. For MALDI experiments, ZnO-OA (12 mg/mL in THF) and ZnO-PSAN (40 mg/mL in THF) samples were spotted on top of dried SA depositions to produce the highest ion flux. When ZnO-L and matrix solutions were mixed in the liquid phase, depositions had a noticeable color change and did not produce intact ions. Sample concentrations were estimated based on preparations from dry mass. Samples ionized best at the previously mentioned concentrations. Depositions were ablated with 337 nm radiation using a pulsed nitrogen laser (Spectra-Physics 337201-01, Santa Clara, CA, USA) with a maximum pulse energy of 260 μJ. For most mass spectra, 2000 shots were collected. Laser intensities were attenuated to levels just above ion production threshold levels to minimize fragmentation.

Data Processing

STJ cryodetection MS data was processed in a Mathematica program developed in-house [15]. The *m*/*z* response of the instrument was calibrated using monoclonal IgG multimers. The non-linear energy response of the STJs was calibrated using ZnO-OA nanoparticles analyzed at different acceleration voltages. Through this approach, a seven-point curve of measured STJ energy response versus ion kinetic energy was fit to a second order polynomial with an r^2 value > 0.99 (see Supplementary Materials).

Results and Discussion

Synthesized ZnO-OA and ZnO-PSAN nanoparticles were previously characterized by traditional non-MS techniques: X-ray diffraction (XRD), transmission electron microscopy (TEM), dynamic light scattering (DLS), and thermogravimetric analysis (TGA) similar to the previous report by Wang et al. [14]. Results from these traditional characterization techniques can be found in the Supplementary Materials. ZnO-OA nanoparticles were found to have average core diameters of 5.2 ± 0.8 nm, based on TEM analysis on 93 individual particles. ZnO-PSAN nanoparticles were found to have average core diameters of 5.4 ± 0.9 nm, based on TEM analysis of 97 particles. TGA results suggested that ZnO-OA and ZnO-PSAN nanoparticles were comprised of 81% and 70% wt inorganic material, respectively. Through knowledge of the size, density, molecular weight, and relative mass contribution of core/ligand materials, grafting densities (σ) [16], that is, the ligand-loadings on the surface of the nanoparticles, were calculated. Using these results, σ_{trad} values were determined to be 5.3 and 0.9 nm^{-2} for ZnO-OA and ZnO-PSAN nanoparticles, respectively [14].

Cryodetection MS was next used to study the composition of synthesized ZnO nanoparticles. By measuring intact

molecular weights, MS may be able to provide more exact determinations of nanoparticle size and composition. MS analysis is also rapid since the analyses are done in the gas phase and it provides quality statistics since thousands of ions make up the data. A 3D MALDI-TOF-STJ mass spectrum of ZnO-OA nanoparticles is shown in Figure 1a. The data shown highlight the additional detection capabilities of STJ MS, where the energies deposited by impacting particles are measured in addition to m/z. In Figure 1a, intact ZnO-OA particles were detected as singly charged species with the apex of the mass distribution (M_p) at 600 kDa. The full width at half maximum (FWHM) of this singly charged distribution was 780 kDa, which describes a broad mass dispersity of these nanoparticles arising from varying numbers of Zn and O atoms in the core and also the variability of the number of ligands attached to the surface. A significant broad peak of near equal ion abundance was detected at an energy level below that of the singly charged species as shown in Figure 1b. This broad peak with M_p at 630 kDa was assigned to products from metastable fragmentation of the ZnO-L precursor ions. Since fragmentation occurs post-acceleration, these ions are not mass analyzed directly by TOF. Instead, metastable fragments are detected at m/z values corresponding to the parent ion, but at lower energy levels reflecting the partitioning of energy with mass [$m_{product} = m^*_{parent}$ ($E_{product}/E_{parent}$)].

Even when protected by ligands that are expected to have weak ionization efficiencies, these ZnO-L nanoparticles produced intense signals by both LDI and MALDI. It is important to note that nanoparticles are typically coated with protecting ligands to ensure stability and prevent aggregation in solution. The strong absorption of ZnO below 400 nm may provide the energy requirements for extensive desorption, ionization, and fragmentation. LDI-TOF-STJ MS results from the analysis of ZnO-OA nanoparticles are shown in Figure 2. LDI experiments showed reduced m/z values for intact ZnO nanoparticles and an absence of a lower energy metastable fragment signal. These results are consistent with the conclusion that LDI imparts more energy into the nanoparticles causing extensive in-source fragmentation resulting in ligand removal and partial ZnO core dissociation prior to ion acceleration. The M_p of the ZnO-OA signal from the LDI analysis was detected at 160 kTh,

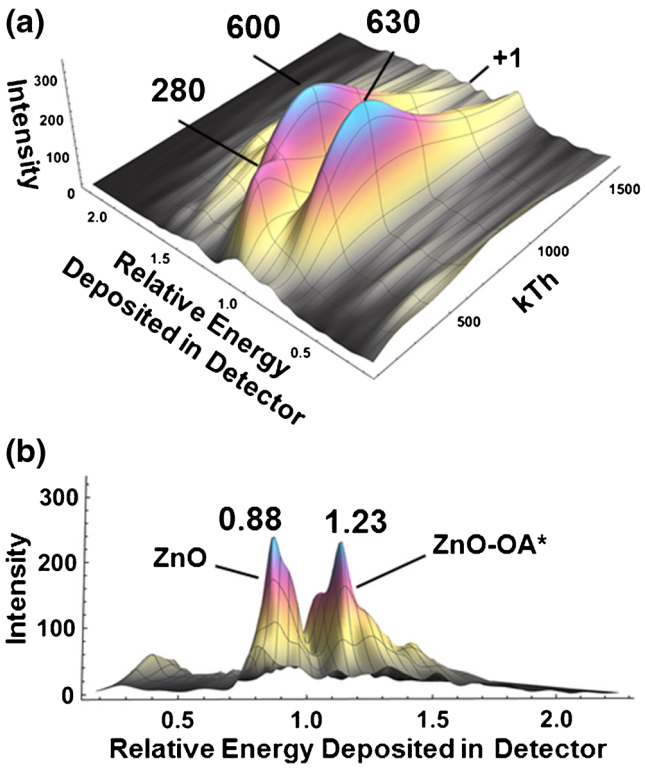

Figure 1. (**a**) 3D MALDI-TOF-STJ MS mass and energy spectrum generated by the analysis of ZnO-OA using sinapinic acid as matrix. The broad peak at 600 kTh represents ZnO-OA at the singly charged energy level. The broad peak at 630 kTh has been assigned to ZnO core fragments resulting from ligand dissociation by metastable fragmentation in the flight tube. (**b**) STJ energy spectrum of ZnO-OA as viewed from the energy axis in (**a**). Two distinct peaks at different energy levels are observed. The peak at the higher arbitrary energy (1.23) has been assigned as ZnO-OA. The peak at lower arbitrary energy levels (0.88) has been assigned to ZnO cores that lost OA ligands. The asterisk (*) denotes ions, which may undergo metastable fragmentation

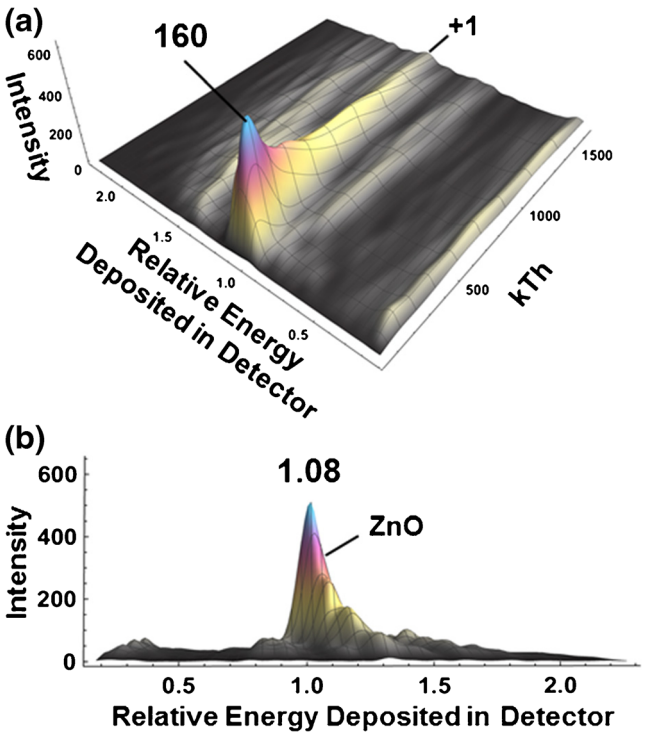

Figure 2. (**a**) 3D LDI-TOF-STJ MS mass and energy spectrum generated by the analysis of ZnO-OA nanoparticles. A sole singly charged peak was observed at 160 kTh, a shift towards lower m/z from 600 kTh in Figure 1 (MALDI), which has been assigned to predominately ZnO cores after loss of ligands and some core material by in source fragmentation during the LDI process. (**b**) STJ energy spectrum of ZnO-OA as viewed from the energy axis in (**a**). For LDI-TOF-STJ MS analyses, no low energy metastable fragment peaks were observed, indicating that most dissociation occurs in the ion source rather than through metastable fragmentation post ion acceleration

as shown in Figure 2a. Assuming that all ligands have dissociated via in-source fragmentation during the LDI process, this *m*/*z* determination should correspond to an average ZnO core size of ~4.5 nm in diameter, much smaller than the 5.2 ± 0.8 nm sizes measured by TEM. These results serve as evidence that some additional core material is fragmenting from the nanoparticles during LDI.

Observation of a distinct, well-resolved lower energy peak in Figure 1 suggested that ZnO-OA nanoparticles were fragmenting to a stable product. After correcting for nonlinear responses of the STJ detectors (see Supplementary Materials), a metastable fragment mass was assigned. Through this STJ energy measurement, it was determined that the low energy signal was ~62% of the mass of the parent ion mass distribution. We hypothesized that this mass difference was a result of primarily OA ligand dissociation from intact ZnO-OA as a result of metastable fragmentation in the flight tube. The energy resolution was not high enough to conclusively state whether all ligands were dissociated from the core or whether small pieces of ZnO were also removed. In any regard, the resolved energy peak suggests that fragmentation is occurring to a product that is stable during the remaining mass analysis timescale (<2.7 ms).

In a similar approach, MALDI-TOF-STJ MS was used to characterize ZnO-PSAN nanoparticles. The result from this analysis is shown in Figure 3. Figure 3a shows the 3D-mass and energy spectrum from the analysis of ZnO-PSAN. Intact singly charged nanoparticles were detected with the M_p of the mass distribution of 520 kDa and a broad FWHM of 750 kDa. Again, a lower energy peak was observed, which has been assigned as predominately ZnO cores as a result of ligand stripping of PSAN. For these ZnO-PSAN nanoparticles, the low energy peak was determined to be ~68% of the mass of the intact ZnO-PSAN parent ions. PSAN ligands appear to be bound more strongly to the ZnO core compared with the OA binding to ZnO as shown by the lower relative abundance of ~50% of the metastable fragment peak in Figure 3. This binding strength is also supported by TGA analysis. It should be noted that the ligands arising from the metastable fragmentation of ZnO-L nanoparticles are not observed at low energies in the STJ mass spectra. Since the mass contribution of a single ligand is less than 0.3% of the intact nanoparticle mass, and is well below the energy detection limit of this STJ mass spectrometer, the signal was not observed. It is intriguing that the relative energy deposited into the STJ detector was 1.23 and 1.14 for ZnO–OA and ZnO–PSAN analyzed by MALDI and 1.08 for ZnO-OA and ZnO-PSAN nanoparticles analyzed by LDI. These differences are currently being investigated and will be discussed in a future paper about ion energy deposition into STJs.

LDI-TOF-STJ MS analyses were also performed on ZnO-PSAN nanoparticles and results are shown in Figure 4. LDI experiments showed reduced *m*/*z* values for ZnO nanoparticles and an absence of a lower energy metastable fragment

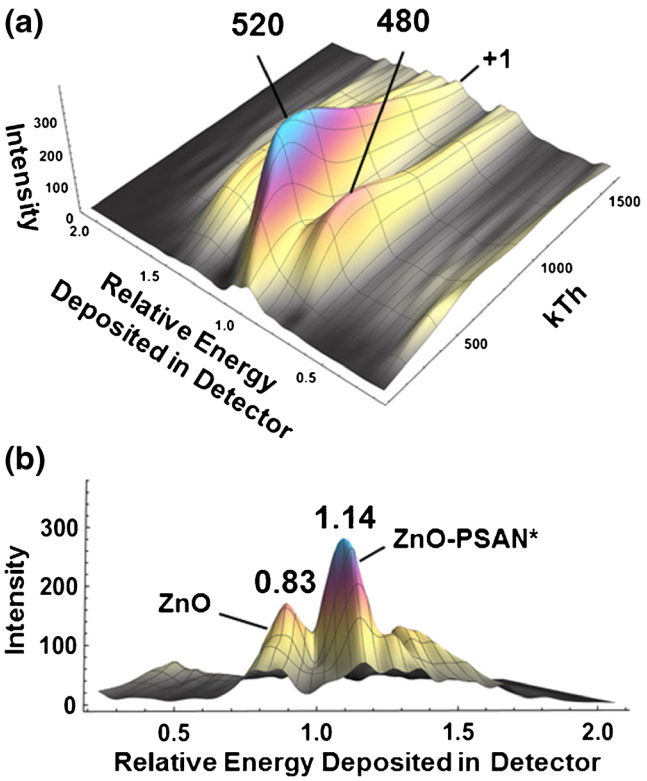

Figure 3. (**a**) MALDI-TOF-STJ MS 3D-mass and energy spectrum generated by the analysis of ZnO-PSAN using sinapinic acid. The peak at 520 kTh represents ZnO-PSAN at the higher singly charged energy level. The peak at half the relative abundance at 480 kTh has been assigned to ZnO core fragments resulting from ligand dissociation during metastable fragmentation. (**b**) STJ energy spectrum of ZnO-PSAN as viewed from the energy axis in (**a**). Two distinct features at different energy levels are observed. The feature at the higher arbitrary energy (1.14) has been assigned as ZnO-PSAN. The feature at lower arbitrary energy levels (0.83) has been assigned to ZnO cores that lost PSAN ligands. The asterisk (*) denotes ions that may undergo metastable fragmention

signal, similar to LDI experiments performed on ZnO-OA nanoparticles as shown in Figure 2. The M_p of the ZnO-PSAN signal from the LDI analysis was detected at 230 kTh, which was assigned to ligand-free ZnO cores with an average size of 5.0 nm. Again, these are smaller than sizes measured by TEM (i.e., 5.4 ± 0.9 nm), as expected, although much closer than those calculated from the LDI analysis of ZnO-OA, providing additional support that the ZnO-PSAN is more robust compared with ZnO-OA nanoparticles. Higher energy signals were also observed in LDI-TOF-STJ MS experiments on ZnO-PSAN nanoparticles. These signals had peak *m*/*z* values of 380 and 410 kTh and have been tentatively assigned to simultaneous multiple particle impacts arising from high ion fluxes to the detector.

While metastable fragments at lower energies are detected at *m*/*z* values identical to that of the parent ions, differences in the most abundant species were observed. Figure 1a shows that for ZnO-OA, metastable fragments at lower energy show increased

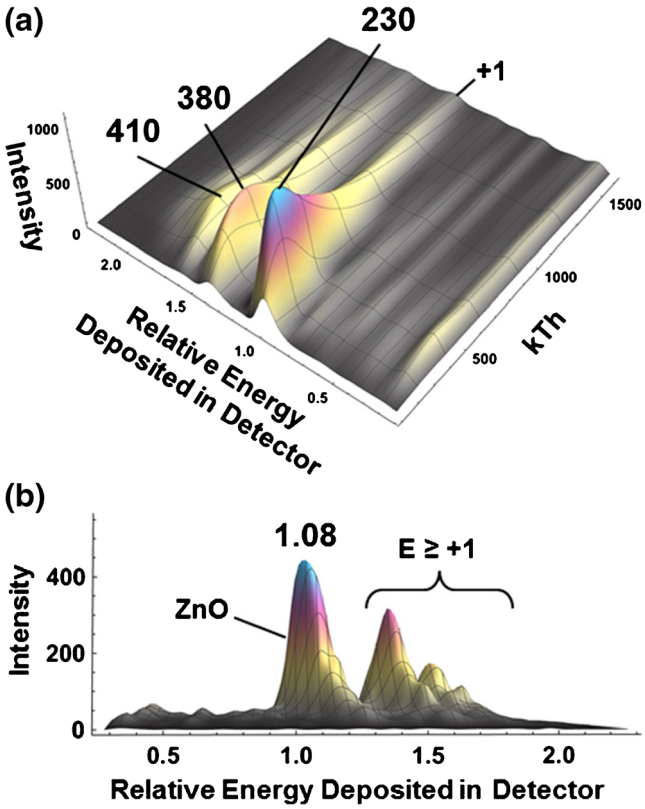

Figure 4. (**a**) 3D LDI-TOF-STJ MS mass and energy spectrum generated by the analysis of ZnO-PSAN nanoparticles. A single singly charged peak was observed at 230 kTh, which is a shift towards lower *m/z* from 520 kTh in Figure 3 (MALDI). This peak was assigned to predominately ZnO cores after loss of ligands and some core material by in-source fragmentation during the LDI process. (**b**) STJ energy spectrum of ZnO-OA as viewed from the energy axis in (**a**). For LDI-TOF-STJ MS analyses, no low energy metastable fragment peaks were observed; however, higher energy signals at 380 and 410 kTh were detected. These signals have been tentatively assigned to simultaneous multiple particle impacts due to high ion flux

abundance for larger molecular weight parent ions. In contrast, Figure 3a shows that for ZnO-PSAN, metastable fragments show an increased abundance for lower molecular weight parent ions. Due to the limited *m/z* resolution, individual ZnO and/or ligand species cannot be resolved. Previous studies in our lab have shown the adduction of ligands and nanoparticle core species and that these adducts can disassociate metastably prior to detection on an STJ [17]. We suspect that some minor contribution to the *m/z* assignment of intact and metastable distributions in Figures 1 and 3 could be affected by differences in adduction of core/ligand fragments. The asymmetric peak shape of intact ZnO-L nanoparticles with tailing towards higher *m/z* also suggested that some adduction was occurring.

Table 1 provides a comparison of analytical characterizations made on ZnO-OA and ZnO-PSAN nanoparticles using MALDI-TOF-STJ MS to more traditional techniques of TEM, TGA, and XRD. MALDI-TOF-STJ MS provided intact mass measurements for ZnO-L nanoparticles, where the most abundant ZnO-OA and ZnO-PSAN species were observed at 600 and 520 kDa, respectively. Assuming that low energy signals observed in STJ MS experiments resulted from only ligand dissociation via metastable fragmentation, we determined that ZnO core average molecular weights were 370 and 350 kDa for ZnO-OA and ZnO-PSAN, respectively. XRD analysis confirmed that the ZnO nanoparticles synthesized were of wurtzite structure and using the estimated core molecular weights, MALDI-TOF-STJ MS calculated ZnO core sizes were found to be 5.9 and 5.8 nm for ZnO-OA and ZnO-PSAN, respectively (see Supplementary Materials). These measurements, based on MALDI-TOF-STJ MS results, are consistent with ZnO core size determinations made by TEM (5.2 ± 0.8 nm and 5.4 ± 0.9 nm for ZnO-OA and ZnO-PSAN, respectively). While 5.2 and 5.4 nm ZnO cores have calculated molecular weights of ~250 and ~280 kDa, respectively, the STJ MS determined core sizes are within one standard deviation. Assuming that no ligand material remained after metastable fragmentation, the STJ MS-based core sizing should be statistically more accurate as the analysis is based on thousands on ions.

In addition to characterizing the size of ZnO-L nanoparticles, we attempted to provide grafting densities based on STJ MS results ($\sigma_{STJ\text{-}MS}$). Assuming that all ligands were removed through metastable fragmentation during the MALDI-TOF-STJ MS analyses, $\sigma_{STJ\text{-}MS}$ for the ZnO cores detected at low energies were calculated to be 16 and 1.1 nm^{-2} for ZnO-OA and ZnO-PSAN, respectively. The $\sigma_{STJ\text{-}MS}$ results for ZnO-OA and ZnO-PSAN were ~3× and ~1.2× higher, respectively, than those calculated by TGA (σ_{trad}). The MS results suggested that the metastable fragmentation of L from ZnO may actually include some ZnO material from the surface of the core. Assuming that one ZnO moiety leaves the core with each

Table 1. Comparison of ZnO Nanoparticle Characterization by MALDI-TOF-STJ Cryodetection MS and Traditional Analytical Techniques (i.e., XRD, TGA, and TEM)

	Particle MW_{avg} (kDa)	% wt Inorganic	Calc. core MW_{avg} (kDa)	Core diameter (nm)	Calc. number ligands	σ (nm^{-2})	Core fragmentation adjusted* $\sigma_{STJ\text{-}MS}$ (nm^{-2})
ZnO-OA (STJ-MS)	600	62%	370	5.9	1800	16	8.6
ZnO-PSAN (STJ-MS)	520	68%	350	5.8	110	1.1	1.0
ZnO-OA (traditional methods)	310	81%	250	5.2	460	5.3	-
ZnO-PSAN (traditional methods)	400	70%	280	5.4	80	0.9	-

*Calculation includes loss of one ZnO per ligand.

ligand removal, the calculated number of molecules tethered to the core becomes 1100 and 110, respectively (77% and 70% wt inorganic), and this gives an adjusted $\sigma_{STJ\text{-}MS}$ values of 8.6 and 1.0 nm^{-2} for ZnO-OA and ZnO-PSAN, respectively (See Table 1). These values are in much better agreement with the TGA results. Low *m/z* LDI and MALDI experiments performed in reflector mode on a higher resolution conventional MALDI-TOF mass spectrometer (Applied Biosystems Foster City, CA, USA, Voyager DE MALDI-TOF-sSTR) showed the presence of free Zn and OA ions, particularly for LDI analyses, indicating that some inorganic species were dissociating from the core during the ionization processes. In the low *m/z* MALDI experiments, a multitude of low mass peaks were observed but assignment was not possible. It is, however, likely that some of these peaks mixed with matrix ions corresponded to Zn containing species (see Supplementary Materials).

Conclusions

Results from this study demonstrate the advantages of using MALDI-TOF-STJ cryodetection MS for the characterization of large heterogeneous ZnO-L nanoparticles. Using this approach, ZnO-L nanoparticle molecular weights and dispersities were measured intact at high *m/z* values (>500 kTh) and with low charge states. In addition, based on metastable fragmentation, a method for determining ligand-loading (grafting densities, $\sigma_{STJ\text{-}MS}$) was presented and ZnO core sizes were explored.

MALDI TOF STJ cryodetection should afford advantages for studying other large, heterogeneous systems while maintaining high sensitivity at high *m/z* and provide additional information about particle compositions and stability through energy analysis of metastable fragments.

Acknowledgements

M.E.B. thanks the National Science Foundation for funding under grant DBI 0454980 and for continued funding under CHE 1611146. The authors acknowledge support of Fan Wang and Jonathan Feldman for Mathematica programming. K.M. acknowledges the National Science Foundation support DMR 1501324.

References

1. Wang, Z.L.: Zinc oxide nanostructures: growth, properties and applications. J. Phys. Condens. Matter. **16**, R829–R858 (2004)
2. Rajalakshmi, M., Arora, A.K., Bendre, B.S., Mahamuni, S.: Optical phonon confinement in zinc oxide nanoparticles. J. Appl. Phys. **87**, 2445–2448 (2000)
3. Becheri, A., Durr, M., Lo Nostro, P., Baglioni, P.: Synthesis and characterization of zinc oxide nanoparticles: application to textiles as UV-absorbers. J. Nanoparticle Res. **10**, 679–689 (2008)
4. Beek, W.J.E., Wienk, M.M., Janssen, R.A.J.: Efficient hybrid solar cells from zinc oxide nanoparticles and a conjugated polymer. Adv. Mater. **16**, 1009–1013 (2004)
5. Twerenbold, D., Vuilleumier, J., Gerber, D., Tadsen, A., van den Brandt, B., Gillevet, P.M.: Detection of single macromolecules using a cryogenic particle detector coupled to a biopolymer mass spectrometer. Appl. Phys. Lett. **68**, 3503–3505 (1996)
6. Twerenbold, D., Gerber, D., Gritti, D., Gonin, Y., Netuschill, A., Rossel, F., Schenker, D., Vuilleumier, J.L.: Single molecule detector for mass spectrometry with mass independent detection efficiency. Proteomics **1**, 66–69 (2001)
7. Westmacott, G., Frank, M., Labov, S., Benner, W.: Using a superconducting tunnel junction detector to measure the secondary electron emission efficiency for a microchannel plate detector bombarded by large molecular ions. Rapid Commun. Mass Spectrom. **14**, 1854–1861 (2000)
8. Ozdemir, A., Aksenov, A.A., Firek, B.A., Hendrix, R.W., Bier, M.E.: The analysis of biomacromolecules using a MALDI TOF mass spectrometer incorporating a superconducting tunnel junction (STJ) cryodetector. Proceeding of the 55th ASMS Conference on Mass Spectrometry and Allied Topics, June 2007; Indianapolis, IN, USA (2007)
9. Aksenov, A.A., Bier, M.E.: The analysis of polystyrene and polystyrene aggregates into the mega dalton mass range by cryodetection MALDI TOF MS. J. Am. Soc. Mass Spectrom. **19**, 219–230 (2008)
10. Wenzel, R.J., Matter, U., Schultheis, L., Zenobi, R.: Analysis of megadalton ions using cryodetection MALDI time-of-flight mass spectrometry. Anal. Chem. **77**, 4329–4337 (2005)
11. Plath, L.D., Ozdemir, A., Aksenov, A.A., Bier, M.E.: Determination of iron content and dispersity of intact ferritin by superconducting tunnel junction cryodetection mass spectrometry. Anal. Chem. **87**, 8985–8993 (2015)
12. Epifani, M., Arbiol, J., Diaz, R., Peralvarez, M.J., Siciliano, P., Morante, J.R.: Synthesis of SnO2 and ZnO colloidal nanocrystals from the decomosition of Tin(II) 2-ethylhexanoate and zinc(II) 2-ethylhexanoate. Chem. Mater. **17**, 6468–6472 (2005)
13. Weber, D., Botnaras, S., Pham, D.V., Steiger, J., De Cola, L.: Functionalized ZnO nanoparticles for thin-film transistors: support of ligand removal by non-thermal methods. J. Mater. Chem. C **1**, 3098–3103 (2013)
14. Wang, Z., Mahoney, C., Yan, J., Lu, Z., Ferebee, R., Luo, D., Bockstaller, M.R., Matyjaszewski, K.: Preparation of well-defined poly(styrene-co-acrylonitrile)/ZnO hybrid nanoparticles by an efficient ligand exchange strategy. Langmuir **32**, 13207–13213 (2016)
15. Sipe, D.M., Wang, F., Duda, R.L., Hendrix, R.W., Bier, M.E.: 3D-histograms improve visualization and charge state determination from macromolecular STJ cryodetection MS Data. Proceeding of the 61st ASMS Conference on Mass Spectrometry and Allied Topics, June 2013; Minneapolis, MN, USA (2013)
16. Benoit, D.N., Zhu, H., Lilierose, M.H., Verm, R.A., Ali, N., Morrison, A.N., Fortner, J.D., Avendano, C., Colvin, V.L.: Measuring the grafting density of nanoparticles in solution by analytical ultracentrifugation and total organic carbon analysis. Anal. Chem. **84**, 9238–9245 (2012)
17. Plath, L.D., Zeng, C., Chen, Y., Jin, R., Bier, M.E.: Tandem MS of synthetic nanoparticles through analysis of metastable fragments using MALDI-TOF MS with superconducting tunnel junction cryodetection. Proceedings of the 64th ASMS Conference on Mass Spectrometry and Allied Topics, June 2016; San Antonio, TX, USA (2016)